Universidad Carlos III de Madrid
e-Archivo

Institutional Repository

This document is published in:

Solar Energy Materials and Solar Cells (2013).109, 185-191.
DOI: http://dx.doi.org/10.1016/j.solmat.2012.10.021

© 2012 Elsevier B.V.

Flow, thermal and structural application of Ni-foam as volumetric solar receiver

N. Michailidis [a,1], F. Stergioudi [a,1], H. Omar [a,1], D. Missirlis [b,n], Z. Vlahostergios [b], S. Tsipas [c], C. Albanakis [b], B. Granier [d]

[a] Department of Mechanical Engineering, Physical Metallurgy Laboratory, Aristotle University of Thessaloniki, Thessaloniki 54124, Greece
[b] Department of Mechanical Engineering, Laboratory of Fluid Mechanics and Turbomachinery, Aristotle University of Thessaloniki, Thessaloniki 54124, Greece
[c] Department of Materials Science and Engineering, Universidad Carlos III de Madrid, Avda de la Universidad, 28911 Leganes, Spain
[d] PROMES-CNRS, 7 rue du four Solaire, 66120 Odeillo Font-Romeu, France
* Corresponding author. Tel.: +30 2310 996033; fax: +30 2310 996002. E-mail address: misirlis@eng.auth.gr (D. Missirlis).
[1] Tel.: +30 2310 995891; fax: +30 2310 996069.

Abstract: Open-cell nickel foams with 92% porosity and uniform pore size and distribution were used in this study. The main objective of this work was to evaluate the behaviour of Ni-foam, when treated as volumetric receivers under concentrated solar radiation while improving their oxidation resistance, in order to make them attractive for such applications. The experimental investigation showed that their efficiency was depending on both materials parameters and flow conditions, the latter affecting the pressure drop and the heat transfer behaviour. The microstructural characterisation of oxide surface morphologies formed on the open-cell Ni foams exposed to concentrated solar radiation is investigated by the use of SEM and EDXS. SEM observations revealed a rapid homogeneous oxidation in the Ni-foam with three different surface oxide structures formed in relation with the process temperature. A novel slurry-based process for aluminising nickel foams while retaining their geometrical properties is applied in order to develop an aluminide–nickel intermetallic coating on a Ni foam thus enhancing the oxidation resistance. Scanning electron microscopy and X-ray diffraction were applied to assess the effectiveness of the aluminising process and determine the optimum parameters of the procedure (slurry composition, holding temperature and time).

Keywords: Ni foam, Volumetric receivers, Solar radiation, Slurry aluminising, Pressure drop, Heat transfer

1. Introduction

Metal foams can be used in many industrial applications ranging from thermal insulation and electromagnetic shielding to energy absorption during impact [1,2]. They are also well-suited for heat exchange applications [3,4] since their open cell structure ensures a high surface area, while the pressure drop remains limited, especially for high-porosity foams [5]. These applications require both high mechanical performance as well as resistance to corrosion and high temperature oxidation. Although several papers have been published on the use of metal foams as heat exchangers, their potential application as volumetric solar receivers is rarely investigated [5–8]. Despite the good thermal conductivity of metal foams as well as their excellent ductility, the main restriction in their application as volumetric solar receivers is the stability of porous metals at high temperatures. Ni foams possess high thermal stability and the potential to coat them for further increasing oxidation resistance [6] is among the benefits for investigating their application as volumetric solar receiver.

Additionally, little effort has been devoted to the morphological and microstructural oxidation phenomena taking effect on the surface of the metal foam especially when exposed to concentrated solar radiation. Therefore, there is a fundamental interest in better understanding and controlling the basic procedure parameters leading to certain oxide morphologies.

It is well known that unalloyed nickel exhibits poor resistance to hot corrosion. A possible improvement while conserving the properties of the metal can be achieved through the development of intermetallic Ni compound foams [9–11] as the developed Ni-aluminides are known to have excellent high-temperature, oxidation and corrosion resistance properties [12,13]. Ni aluminides have been produced using different methods, for developing protective coatings on Ni-base alloys [10,13–15]. However, lately there has been a trend to develop a simpler and more effective method for such a coating production through the use of a slurry [9,15,16].

2. Materials used and experimental methods

High purity open-cell nickel foams with a porosity of 92% and a mean pore size of approximately 0.6 mm were used in this study. As shown in Fig. 1a the Ni-foam exhibits homogeneous structure and geometrical parameters with regard to cell size,

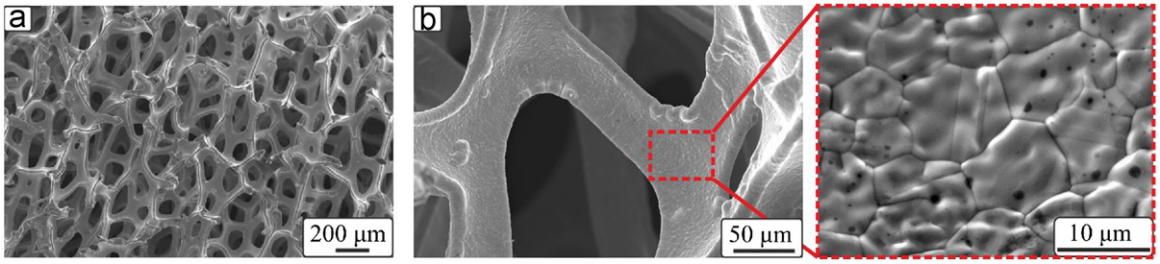

Fig. 1. SEM images depicting (a) a macroscopic view of the cell and (b) the microstructural morphology of the as received Ni-foams.

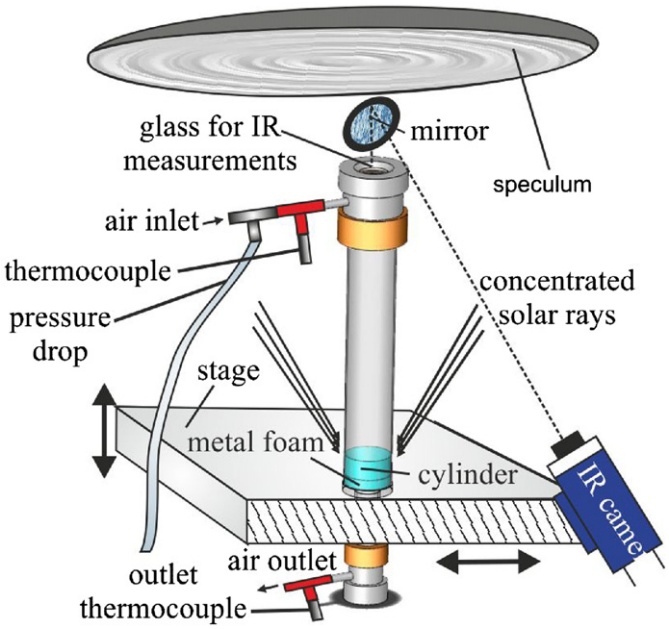

Fig. 2. Experimental apparatus for the examination of Ni-foams under concentrated solar radiation.

strut width and strut wall thickness. The Ni foam was supplied by INCO in the form of a 2 mm thick foil from which circular specimens were cut having a 45 mm diameter. The foams were produced by metal deposition on a polymer pre-form followed by a sintering process.

In order to investigate the foam materials behaviour under concentrated solar radiation combined with the effect of variable gas flow conditions, the experimental setup presented in Fig. 2, was developed. A 2 kW solar concentrator was applied for the experiments, which took place in the facilities of Procedes, Materiaux et Energie Solaire of the Centre national de la Recherche Scientifique (PROMES-CNRS). In the experimental measurements, the static pressure drop between the gas inlet and outlet was measured, together with the gas inlet and outlet temperature. In addition, the mass flow through the foam specimen was measured since this parameter was particularly important for the quantification of the pressure drop and heat transfer performance of the metal foam under investigation. For the estimation of the foam temperature, an IR camera was used during the test. During the measurements, the specimen temperature was adjusted and controlled by raising or lowering the stage, where the whole setup was mounted. Thus, the distance of the "hot-spot" from the specimen and, thus, its temperature could be modified and controlled, for given gas flow parameters. The specimen was mounted inside the experimental setup within two cement holders. The top holder had a conical shape in order to allow for a more uniform gas flow distribution which would lead to more representative results regarding the foam flow and thermal performance. For the evaluation of the performance of the specimen in relation to flow conditions, pressure drop and temperature measurements were performed between the inlet and the outlet of the experimental setup. The pressure drop measurements were performed with the use of a Bioblock Scientific MP330, digital manometer connected to the air supply right before the inlet of the experimental setup while the outlet was kept at ambient pressure. Three flow rates were measured for each foam specimen corresponding to approximately 50%, 80% and 100% of the maximum available mass flow rate of the air supply, which was equal to 30 l/min. The mass flow rate was measured with the use of a Brooks Mass Flow Controller, 5850E. The pressure drop and temperature measurements were performed for a varying distance of the focal point in order to obtain data of the pressure drop and thermal behaviour for a varying surface temperature of the foam specimen, which was measured with a Flir Systems, SC100 thermo camera. Finally, the air outlet temperature was measured with the use of a thermocouple connected at the outlet of the experimental setup. Regarding its applicability as a volumetric receiver, it must be mentioned that approximately 12.5% of the incident light passes through the 2 mm thick foam. More details about the experimental set-up can be found in [5].

The microstructural characterisation of oxide surface morphologies formed on Ni foams exposed to concentrated solar radiation is investigated by the use of scanning electron microscopy (SEM) and EDS. A JEOL JSM-5900LV scanning electron microscope equipped with an energy dispersive X-ray spectrometer was utilised.

In order to reduce the oxidation phenomenon, a simple, one-step slurry process was carried out to aluminise the nickel. The process initially involves the immersion of the samples of the unalloyed as received Ni-foam in the slurry of the activating element to be diffused and subsequently the heating at appropriate temperature levels and adequate process duration in order to obtain a uniform modified surface layer at the struts of the foam. Several slurries of different compositions were examined to investigate the possibility of developing an aluminide–nickel intermetallic coating on Ni foam without affecting the original structural properties of the foam. The phases formed by the aluminising slurry process were identified by energy dispersive spectroscopy (EDS) as well as by X-ray diffraction analysis (XRD). Aluminisation was conducted under argon atmosphere with the embedded slurry samples heated in a three zone tube furnace. The samples were then allowed to cool at room temperature under the argon atmosphere. The slurries used in this study consist of the activating compound, inert alumina powder, an organic binder and two halide salts, ammonium chloride (NH_4Cl) and aluminium chloride ($AlCl_3$) in different proportions while the process temperature was varying from 400 to 850 °C and the process holding time was ranging between 2 h and 6 h.

3. Results and discussion

3.1. Flow and thermal properties

For the investigation and the assessment of the flow and thermal properties of the metal foam, the pressure drop and the heat transfer were measured. For this reason the static pressure drop between the gas inlet and outlet together with the gas inlet and outlet temperature were measured. The measurements were performed for one and two metal foam specimens placed in a row in order to assess the effect of the metal foam thickness on the pressure drop. The experimental measurements were analysed based on the mean conditions of the air flow velocity and density which are corresponding to the mean air flow temperature between inlet and outlet. The static pressure drop measurements are presented in Figs. 3 and 4. The experimental measurements show that the pressure drop can be sufficiently described by a second order polynomial trend line similar to the Darcy–Forchheimer pressure drop law which is as follows:

$$\frac{\Delta P}{L} = \frac{\mu}{K}V + \rho C V^2 \tag{1}$$

where ΔP is the static pressure drop, L is the length of the porous medium, μ is the dynamic viscosity, K is the permeability, V is the mean air flow velocity, ρ is the mean air flow density and C is the form drag coefficient.

The pressure loss coefficients C and K can be derived from a trend line curve fitting procedure between the experimental data and the Darcy–Forchheimer pressure drop law formula. The experimental measurements show clearly the effect of the temperature on the static pressure drop. As it can be seen, the higher the mean air flow temperature is, the higher the pressure drop between the inlet and the outlet of the metal foam specimen will be. Similar behaviour is also presented in the work of Albanakis et al. [17] and Missirlis et al. [18] where the static pressure drop through a heat exchanger for aero engine application was investigated experimentally and then analysed in order to derive a porous medium model capable of describing the macroscopic pressure drop behaviour of the heat exchanger core (consisting of elliptic tubes in a staggered arrangement) which was later used for CFD computations. A similar approach can be presented in the future for the experimental measurements presented in this work, in order to develop engineering tools for numerical studies. Since the static pressure drop is directly correlated with the air flow mean temperature, the heat transfer effect of the metal foam

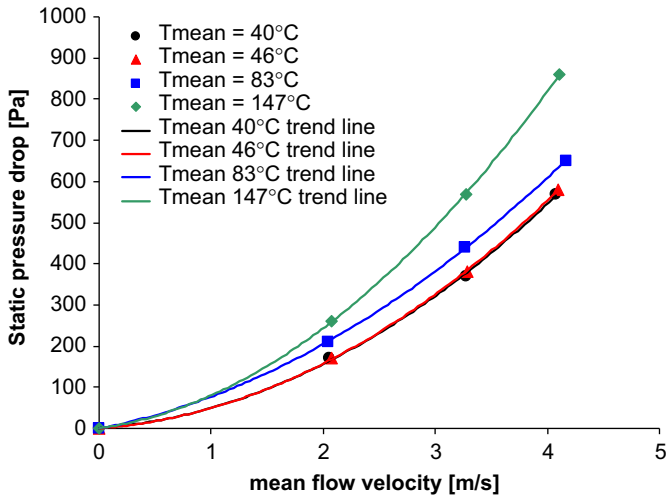

Fig. 3. Static pressure drop towards mean air flow velocity for varying air flow mean temperature (one sample).

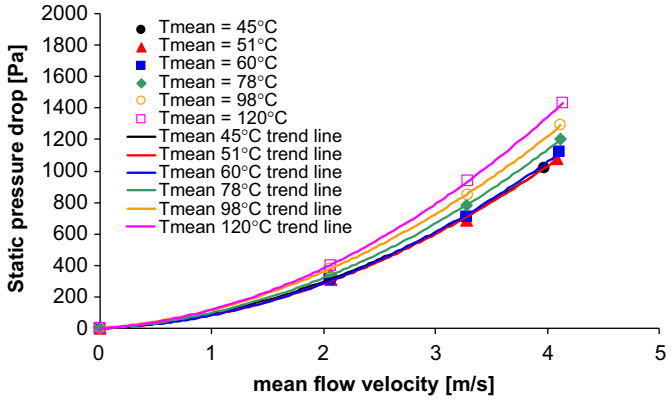

Fig. 4. Static pressure drop towards mean air flow velocity for varying air flow mean temperature (two samples in a row).

specimen should be necessarily taken into consideration since otherwise the air flow mean temperature, density and velocity could not be sufficiently estimated and thus, the static pressure drop will not be accurately predicted. To compensate for this problem, and similarly to the work of Missirlis et al. [18], the heat transfer behaviour of the metal foam specimen can be described by an approach based on the estimation of the Nusselt number of the flow. For the analysis, the experimental results and the metal foam are treated equivalently to a heat exchanger of staggered tube rows in tube bundles. Hence, the heat transferred to the fluid in the pores of the metal foam sample can be characterised by the heat transfer coefficient. By consequence, the Nusselt number presented in the following equation can be defined, based on the mean heat transfer coefficient as:

$$Nu_D = \frac{\overline{h}D}{k} \tag{2}$$

where D is the characteristic length, $\overline{h}$is the heat transfer coefficient and K is the thermal conductivity.

All properties are estimated at the mean air flow temperature between air flow inlet and outlet. Since the cross section of the metal foam strut is not circular, a shape factor for the estimation of the characteristic length, D, has to be taken into account according to Lu et al. [4], given from the following equation as:

$$D = \left(1 - e^{-((1-\varepsilon)/0.04)}\right) d_f \tag{3}$$

where d_f is the strut diameter of the metal foam.

$$\frac{d_f}{d_p} = 1.18\sqrt{\frac{(1-\varepsilon)}{3\pi}}\left(\frac{1}{1-e^{-((1-\varepsilon)/0.04)}}\right) \tag{4}$$

where d_p is the diameter of the pore and ε is the porosity of the metal foam.

At the next step, the Reynolds number is calculated based on the flow velocity in the pore, the characteristic length and the kinematic viscosity, presented in the following equation:

$$\mathrm{Re}_D = \frac{u_{pore}D}{\nu} \tag{5}$$

where $u_{\mathrm{pore}} = u_{\mathrm{fluid}}/\varepsilon$ is the flow velocity in pore and ν is the kinematic viscosity.

Finally, based on the suggestions of Zukauskas [19], for similar setups, the Nusselt number can be estimated as a function of Reynolds number and Prandtl number as:

$$Nu_D = 0.76\mathrm{Re}^{0.4}\mathrm{Pr}^{0.37} \tag{6}$$

It should be mentioned that Eq. (6) is similar to the Nusselt correlation derived from the experimental measurements presented in the work of Missirlis et al. [18] and was used for the

development of a heat transfer model of a heat exchanger for aero engine applications. This correlation is presented in the following equation where a, m and n are constants:

$$Nu_D = \alpha \mathrm{Pr}^m \mathrm{Re}^n \quad (7)$$

In addition, in order to investigate the temperature distribution through the metal foam specimen, CFD computations were performed. For this reason a small part of the foam (of approx. 2 mm × 2 mm × 2 mm dimensions) was captured by computed tomography (CT) and the built geometry was inserted in a rectangular computational domain. At the next step, a computational grid of approximately 1.3 million computational points was created with the ANSYS automated grid generator software utility. Typical views of the computational grid, the computational domain and the applied boundary conditions are presented in Figs. 5 and 6. It must be mentioned that the creation of a detailed CFD model was applied only for a representative volume of the foam and not for the total metal foam region so as to avoid having to create a computational grid of extremely high number of computational points which could lead to unaffordable CPU and memory requirements. The CFD computations were performed with the FLUENT CFD software. The flow was computed as steady and turbulent with air with ideal gas properties being the working fluid. For the turbulence modelling the Realisable k–e turbulence model [20] with enhanced wall treatment was used, with the turbulence intensity estimated at 1%, due to lack of precise experimental measurements. At the inlet of the computational domain the static temperature, the flow velocity and the turbulence intensity were prescribed while at the outlet of the computational domain the value of ambient static pressure was imposed. Regarding the metal foam wall thermal conditions, constant heat flux was applied. The latter was calculated from the experimental measurements through the calculation of the heat exchange taking place between air flow inlet and outlet. Typical views of the air flow field and temperature distribution through the metal foam specimen middle plane are presented in Fig. 7 corresponding to inlet air flow velocity of 1.22 m/s and static temperature of 296 K.

Finally, in order to obtain an inside overview of the temperature distribution through the heat exchanger, the computational domain on the metal foam specimen region was divided into 11 cutting planes for which the area-weighted temperature value of each one was calculated. The results are presented in Fig. 8 in non-dimensional form where T is the air flow static temperature at each plane, T_{inlet} is the air flow static temperature at inlet and T_{outlet} is the air flow static temperature at outlet.

3.2. Oxides morphologies formed on Ni-foam

In order to clarify the surface state of both the high-purity Ni-foam and the Inconel foam prior to oxidation, SEM micrographs of the as received materials were taken. Fig. 1b depicts the microstructure of the as received Ni-foam. The surface of the Ni-foam is rather smooth having only a small number of protruding nodules. A delineation of grain boundaries can be seen in higher magnification SEM images. The grain size is rather uniform and averages about 8–12 μm in diameter. All grain surfaces are

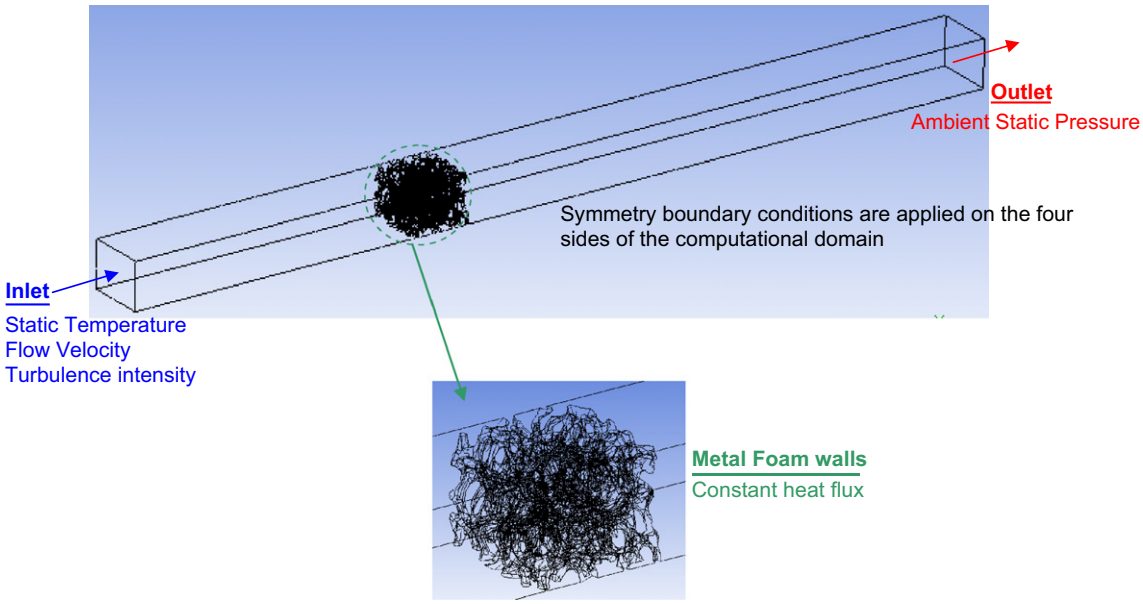

Fig. 5. Computational domain with applied boundary conditions.

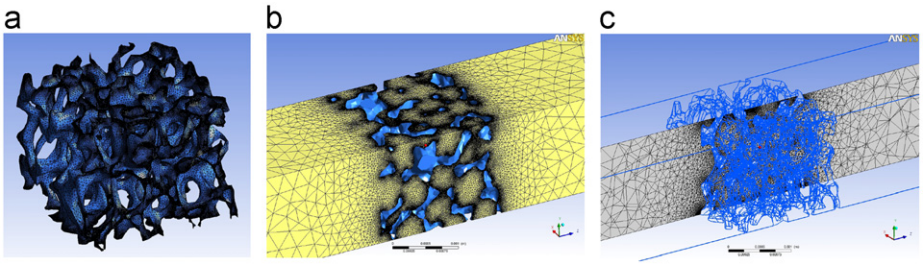

Fig. 6. Views of the computational grid: (a) on metal foam surface; (b) in the proximity of the metal foam region and (c) in the middle cross section of the computational domain.

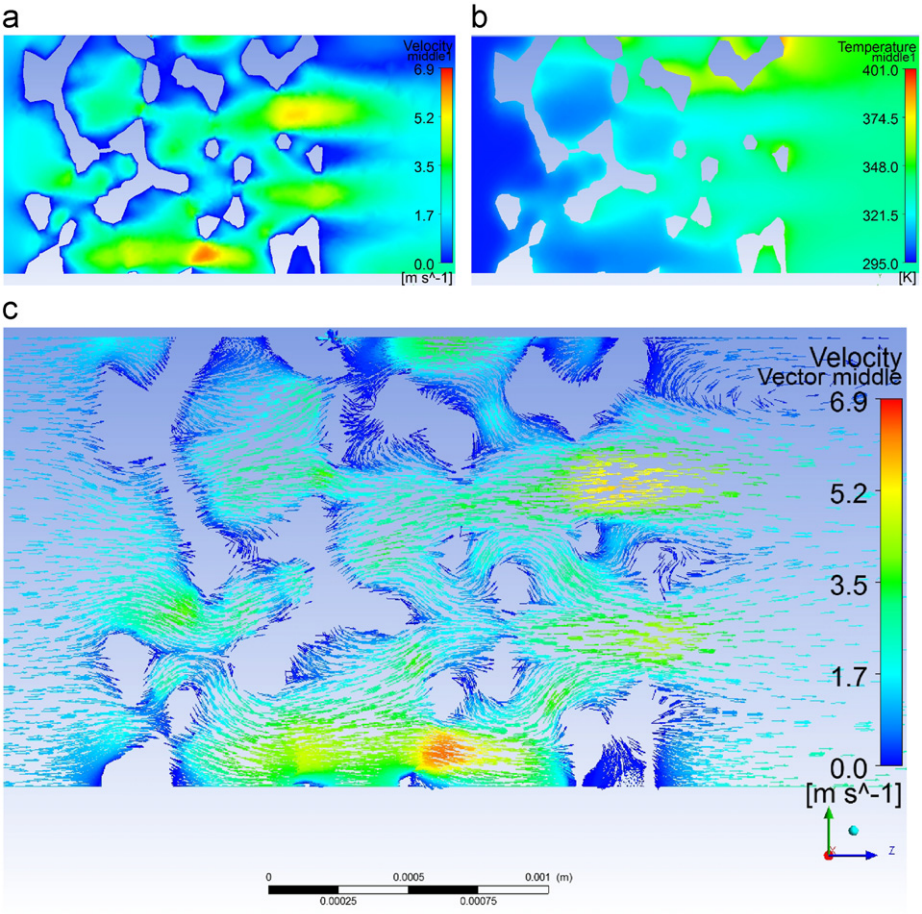

Fig. 7. Flow field and temperature distribution through the middle plane of the metal foam specimen: (a) velocity magnitude; (b) static temperature and (c) velocity vectors.

rounded, with this curvature being more intense in smaller grains. Faceting is also pronounced throughout all the grains of the Ni-foam samples.

Within the investigated ranges of oxidation temperature (200–1100 °C), SEM observations revealed three different surface morphologies of the formed oxide. At low temperatures (200–400 °C), a thin NiO grows retaining the faceted morphology and initial Ni-grain orientations. At temperatures of about 400 °C, isolated oxide particles with irregular shape and size were also observed (Fig. 9a). The occurrence of such isolated particles seems to be independent of nickel-grain orientation or grain boundaries since they are evenly distributed in all grains and are located both in the inner region and the boundaries of the crystallites. EDXS results at the grey background oxide and at the bright oxide particles showed that the O content was the same (about 30 at% or 11 wt%) in both regions indicating that the oxide particles are also thin.

At temperatures between 500 and 700 °C the oxide surface is highly convoluted with protruding, interconnecting ridges distributed all over the sample leaving distinct pores. The most specific features of such NiO are their small grain size and their cellular morphology, which is characterised by numerous open porosities and ridges. Fig. 9b depicts a typical cellular morphology. It seems that the oxide particles grown at low temperatures served as nucleus for the growth of cellular morphology oxides. The coverage of this oxide cellular morphology is adequately uniform. However, locally small regions with limited cellular oxide morphology can be found (Fig. 9c) in which the trace of a nickel-grain boundary is evident (shown by the white arrow),

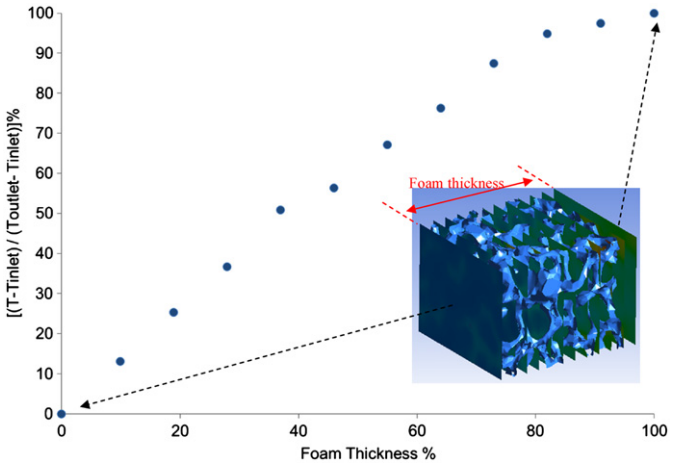

Fig. 8. Temperature distribution through the metal foam thickness.

demonstrating thus that the crystallographic orientation of the underlying nickel-grain does not influence the growth of the oxide.

By increasing the temperature at 800 °C a grain-size refinement of cellular oxide morphology is observed (Fig. 9d). The interconnected ridges are becoming less acute in shape and tend to disappear after a certain time by being progressively buried by the surrounding oxide layer therefore producing a rough morphology, characterised by correlated oxide bumps (Fig. 9e). Further heating at temperatures above 900 °C results in a full

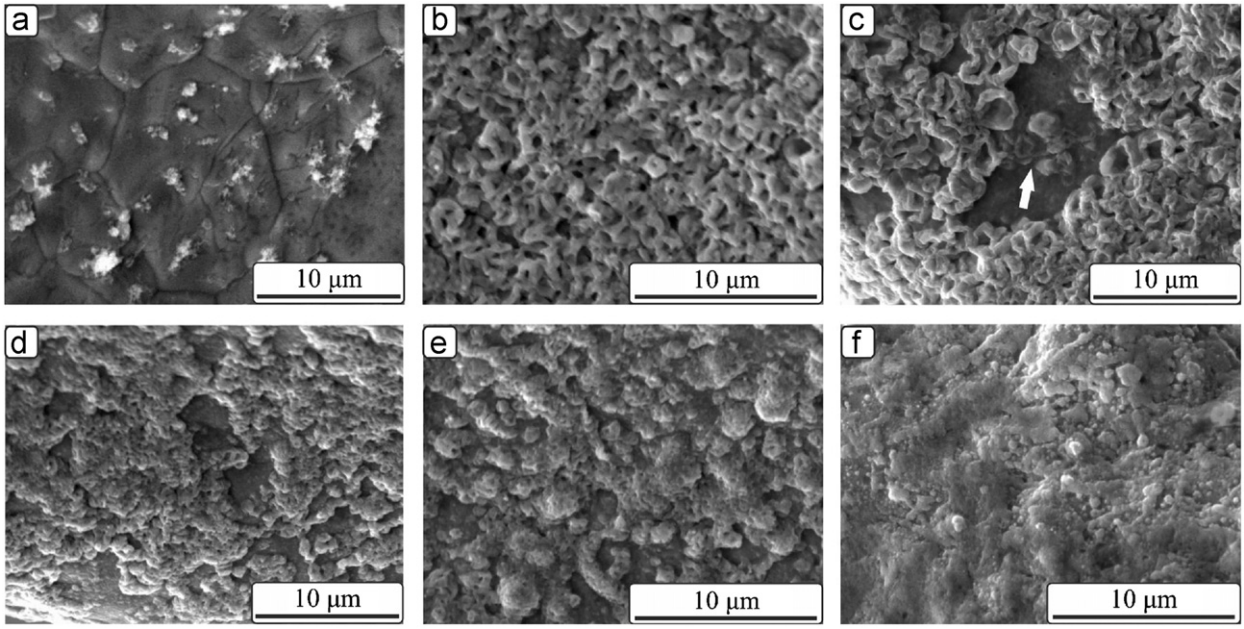

Fig. 9. SEM micrographs of the surface microstructural morphology of the Ni-foam oxidised at (a) 300 °C, (b) and (c) 600 °C, (d) 800 °C, (e) 900 °C and (f) above 900 °C.

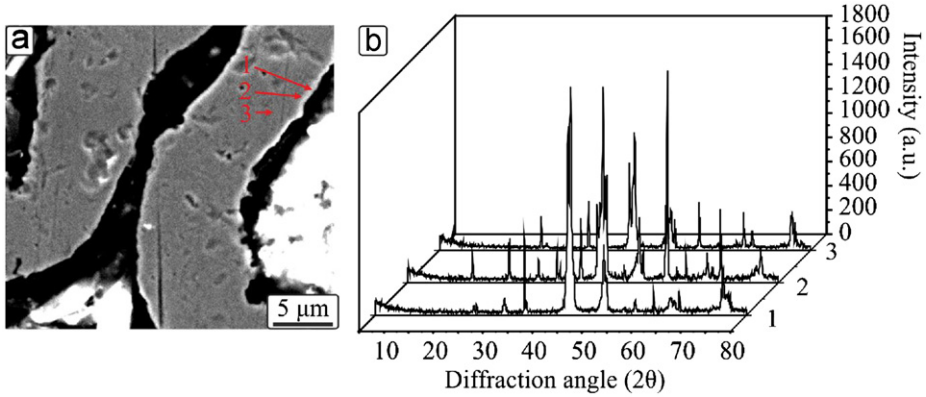

Fig. 10. (a) Characteristic cross-section of two aluminised struts at 400 °C for 6 h, (b) X-ray diffraction pattern using CuKa radiation obtained for the produced aluminised Ni-foams at different process parameters (temperature/holding time). XRD 1: process parameters: 650 °C/2 h, phases identified: Ni_3Al, Ni_5Al_3, NiAl, Ni_2Al_3, XRD 2: process parameters: 500 °C/2 h, phases identified: Ni, Ni_3Al, Ni_5Al_3, NiAl, Ni_2Al_3 and XRD 3: process parameters: 400 °C/4 h phases identified: Ni, Ni_5Al_3, NiAl.

coverage of the metal surface with a bump-like oxide morphology. Such a microstructure could be derived from the lateral growth of the incipient oxide bumps so as to achieve a minimum oxide surface. It is noticeable that for temperatures above 900 °C the oxide structure between the bumps was fairly smooth (Fig. 9f).

3.3. *Slurry aluminisation*

Metallographic cross sectional SEM images of the foams revealed a macroscopic gradient of composition which was initially visible in terms of a clear contrast, indicative of an inner, nickel rich and outer aluminium rich region in the struts of the foams (Fig. 10). The enclosed black area represents the internal cavities of the hollow struts. It can be seen that a zone of two layers (a thick external layer followed by a thin internal layer) is formed in the outer wall surface of the strut. This zone appears uniform and continuous, while elemental microanalysis revealed the existence of Al within the Ni matrix of the foam. Analysis in different depths from the wall surface of the struts indicated the presence of an external Al-rich (14–17 wt%), layer that is followed by a layer of low Al content (2–7 wt%), both constitute the case depth of aluminising. The depth of the bright zone visible around each strut varies with the process parameters of aluminising (temperature, time, slurry composition). The aluminising of the foams did not influence the overall geometry of the foam, e.g. open cells with hollow struts, as their macroscopic size and shape are maintained.

The same layer sequence is visible from the inner wall surface of the strut illustrating that aluminising occurred from both the inner and outer surfaces of the hollow strut. However, the inner layer is noticeably thinner than the outer one, demonstrating thus that the aluminium flux was larger on the outer strut wall surface. The fact that aluminising takes place from within the hollow struts of the foams reveals that there are many openings in the walls of the struts, which were probably created during the removal of the polymer foam after nickel deposition.

Depending on the process temperature and duration, as well as the Al content in the slurry, intermetallic phases as Ni_3Al, Ni_5Al_3, NiAl, Ni_2Al_3 were formed (Fig. 6b). The formation and the percentage of each of these phases within the surface layer can be controlled by proper selection of the process parameters (temperature, duration

and slurry composition). This fact validates the assumption that by choosing either relatively low Al percentages in the slurry used, or low process duration, even a surface layer consisted of (Ni) solid solution could be achieved, as predicted by the Ni–Al equilibrium phase diagram for Al percentages up to 11 wt%.

4. Summary–conclusions

In the present work, an analysis of the flow and thermal behaviour of metal foam specimens was performed. The analysis was based on experimental measurements and literature survey so as to describe the overall performance of the foam specimen in relation to flow and thermal conditions. Furthermore, CFD computations were perfomed on a small part of the foam captured by computed tomography. The experimental measurements showed that the behaviour of the metal foam specimen could be sufficiently treated similarly to the behaviour of a heat exchanger with staggered tubes arrangement. The conclusions which were derived can be used further for the development of a general purpose heat transfer and pressure drop model. The latter can be used for numerical studies in the future in combination with detailed CFD computations, in complicated applications where the foam specimen geometry is modelled as a porous medium with predefined pressure drop and heat transfer behaviour. Additionally, the slurry aluminisation of Ni-foams proved to be a powerful low-temperature surface treatment method for creating oxidation resistant coatings for porous materials. The proposed technique is simple, flexible and easily applicable, allowing additional alloying elements as boron to be added during aluminisation.

Acknowledgements

The authors would like to thank the PROcedes Materiaux et Energie Solaire (PROMES)–Centre National de la Recherche Scientifique (CNRS) for their support in the experimental procedure in the frame of the European Project SOLFACE.

References

[1] M.F. Ashby, A.G. Evans, N.A. Fleck, L.J. Gibson, J.W. Hutchinson, H.N.G. Wadley, Metal Foams: A Design Guide, Butterworth–Heinemann, Oxford, 2000, pp. 150–193.
[2] H.P. Degischer, B. Kriszt, Handbook of Cellular Metals, Production, Processing, Applications, Wiley-VCH, Weinheim, 2002, pp. 179–242.
[3] K. Boomsma, D. Poulikakos, F. Zwick, Metal foams as compact high performance heat exchangers, Mechanics of Materials 35 (2003) 1161–1176.
[4] W. Lu, C.Y. Zhao, S.A. Tassou, Thermal analysis on metal-foam filled heat exchangers Part I: metal-foam filled pipes, International Journal of Heat and Mass Transfer 49 (2006) 2751–2761.
[5] C. Albanakis, D. Missirlis, N. Michailidis, K. Yakinthos, A. Goulas, H. Omar, D. Tsipas, B. Granier, Experimental analysis of the pressure drop and heat transfer through metal foams used as volumetric receivers under concentrated solar radiation, Experimental Thermal and Fluid Science 33 (2009) 246–252.
[6] D. Barlev, R. Vidu, P. Stroeve, Innovation in concentrated solar power, Solar Energy Materials & Solar Cells 95 (2011) 2703–2725.
[7] A.L. Avila-Marın, Volumetric receivers in solar thermal power plants with central receiver system technology: a review, Solar Energy 85 (2011) 891–910.
[8] T. Fend, B. Hoffschmidt, R. Pitz-Paal, O. Reutter, P. Rietbrock, Porous materials as open volumetric solar receivers: experimental determination of thermophysical and heat transfer properties, Energy 29 (2004) 823–833.
[9] H. Omar, D.P. Papadopoulos, S.A. Tsipas, H. Lefakis, Aluminizing nickel foam by a slurry coating process, Materials Letters 63 (2009) 1387–1389.
[10] A.M. Hodge, D.C. Dunand, Synthesis of nickel–aluminide foams by pack-aluminization of nickel foams, Intermetallics 9 (2001) 581–589.
[11] H. Choe, D.C. Dunand, Synthesis, structure, and mechanical properties of Ni–Al and Ni–Cr–Al superalloy foams, Acta Materialia 52 (2004) 1283–1295.
[12] D.B. Miracle, The physical and mechanical properties of NiAl (Overview no. 104), Acta Metallurgica et Materialia 41 (1993) 649–684.
[13] N.S. Stoloff, V.K. Sikka, Physical Metallurgy and Processing of Intermetallic Compounds, Chapman and Hall, New York, 1996, pp. 262–461.
[14] R.D. Noebe, R.R. Bowman, M.V. Nathal, Review of the physical and mechanical properties of the B2 compound NiAl, International Materials Reviews 38 (1993) 193–232.
[15] D.C. Dunand, A.M. Hodge, C. Schuh, Pack aluminisation kinetics of nickel rods and foams, Materials Science and Technology 18 (2002) 326–332.
[16] M.S. Milaniak, D.J. Orzel, F.P. Lamm, D.E. Desaulniers, U.S. Patent 5,366,765, (1994).
[17] C. Albanakis, K. Yakinthos, K. Kritikos, D. Missirlis, A. Goulas, P. Storm, The effect of heat transfer on the pressure drop through a heat exchanger for aero engine applications, Applied Thermal Engineering 29 (2009) 634–644.
[18] D. Missirlis, S. Donnerhack, O. Seite, C. Albanakis, A. Sideridis, K. Yakinthos, A. Goulas, Numerical development of a heat transfer and pressure drop porosity model for a heat exchanger for aero engine applications, Applied Thermal Engineering 30 (2010) 1341–1350.
[19] A.A. Zukauskas, Convective heat transfer in cross-flow, in: S. Kakac, R.K. Shah, W. Aung (Eds.), Handbook of Single-Phase Convective Heat Transfer, Wiley, New York, 1987.
[20] T.-H. Shih, W.W. Liou, A. Shabbir, Z. Yang, J. Zhu, A new-eddy-viscosity model for high Reynolds number turbulent flows—model development and validation, Computers & Fluids 24 (3) (1995) 227–238.